

# Modal and polarization qubits in Ti:LiNbO<sub>3</sub> photonic circuits for a universal quantum logic gate

Mohammed F. Saleh,<sup>1</sup> Giovanni Di Giuseppe,<sup>2,3</sup> Bahaa E. A. Saleh,<sup>1,2,\*</sup> and Malvin Carl Teich<sup>1,4,5</sup>

<sup>1</sup>*Quantum Photonics Laboratory, Department of Electrical & Computer Engineering, Boston University, Boston, MA 02215, USA*

<sup>2</sup>*Quantum Photonics Laboratory, College of Optics and Photonics (CREOL), University of Central Florida, Orlando, FL 32816, USA*

<sup>3</sup>*School of Science and Technology, Physics Division, University of Camerino, 62032 Camerino (MC), Italy*

<sup>4</sup>*Department of Physics, Boston University, Boston, MA 02215, USA*

<sup>5</sup>*Department of Electrical Engineering, Columbia University, New York, NY 10027, USA*

[\\*besaleh@creol.ucf.edu](mailto:besaleh@creol.ucf.edu)

**Abstract:** Lithium niobate photonic circuits have the salutary property of permitting the generation, transmission, and processing of photons to be accommodated on a single chip. Compact photonic circuits such as these, with multiple components integrated on a single chip, are crucial for efficiently implementing quantum information processing schemes. We present a set of basic transformations that are useful for manipulating modal qubits in Ti:LiNbO<sub>3</sub> photonic quantum circuits. These include the mode analyzer, a device that separates the even and odd components of a state into two separate spatial paths; the mode rotator, which rotates the state by an angle in mode space; and modal Pauli spin operators that effect related operations. We also describe the design of a deterministic, two-qubit, single-photon, CNOT gate, a key element in certain sets of universal quantum logic gates. It is implemented as a Ti:LiNbO<sub>3</sub> photonic quantum circuit in which the polarization and mode number of a single photon serve as the control and target qubits, respectively. It is shown that the effects of dispersion in the CNOT circuit can be mitigated by augmenting it with an additional path. The performance of all of these components are confirmed by numerical simulations. The implementation of these transformations relies on selective and controllable power coupling among single- and two-mode waveguides, as well as the polarization sensitivity of the Pockels coefficients in LiNbO<sub>3</sub>.

© 2010 Optical Society of America

**OCIS codes:** (270.5585) Quantum information and processing; (230.7380) Waveguides, channeled; (130.3730) Lithium niobate.

---

## References and links

1. M. F. Saleh, B. E. A. Saleh, and M. C. Teich, "Modal, spectral, and polarization entanglement in guided-wave parametric down-conversion," Phys. Rev. A **79**, 053 842 (2009).
2. M. F. Saleh, G. Di Giuseppe, B. E. A. Saleh, and M. C. Teich, "Photonic circuits for generating modal, spectral, and polarization entanglement," IEEE Photon. J. **2**, 736–752 (2010).
3. M. Fiorentino, S. M. Spillane, R. G. Beausoleil, T. D. Roberts, P. Battle, and M. W. Munro, "Spontaneous parametric down-conversion in periodically poled KTP waveguides and bulk crystals," Opt. Express **15**, 7479–7488 (2007).

4. M. Avenhaus, M. V. Chekhova, L. A. Krivitsky, G. Leuchs, and C. Silberhorn, "Experimental verification of high spectral entanglement for pulsed waveguided spontaneous parametric down-conversion," *Phys. Rev. A* **79**, 043 836 (2009).
5. P. J. Mosley, A. Christ, A. Eckstein, and C. Silberhorn, "Direct measurement of the spatial-spectral structure of waveguided parametric down-conversion," *Phys. Rev. Lett.* **103**, 233 901 (2009).
6. T. Zhong, F. N. Wong, T. D. Roberts, and P. Battle, "High performance photon-pair source based on a fiber coupled periodically poled KTiOPO<sub>4</sub> waveguide," *Opt. Express* **17**, 12 019–12 030 (2009).
7. J. Chen, A. J. Pearlman, A. Ling, J. Fan, and A. Migdall, "A versatile waveguide source of photon pairs for chip-scale quantum information processing," *Opt. Express* **17**, 6 727–6 740 (2009).
8. A. Politi, M. J. Cryan, J. G. Rarity, S. Yu, and J. L. O'Brien, "Silica-on-silicon waveguide quantum circuits," *Science* **320**, 646–649 (2008).
9. J. C. F. Matthews, A. Politi, A. Stefanov, and J. L. O'Brien, "Manipulation of multiphoton entanglement in waveguide quantum circuits," *Nature Photon.* **3**, 346–350 (2009).
10. C. H. Bennett and P. W. Shor, "Quantum information theory," *IEEE Trans. Inform. Theory* **44**, 2724–2742 (1998).
11. M. A. Nielsen and I. L. Chuang, *Quantum Computation and Quantum Information* (Cambridge University Press, Cambridge, UK, 2000).
12. J. L. O'Brien, A. Furusawa, and J. Vučković, "Photonic quantum technologies," *Nature Photon.* **3**, 687–695 (2009).
13. A. Politi, J. C. F. Matthews, M. G. Thompson, and J. L. O'Brien, "Integrated quantum photonics," *IEEE J. Sel. Topics Quantum Electron.* **15**, 1673–1684 (2009).
14. G. Cincotti, "Prospects on planar quantum computing," *J. Lightwave Technol.* **27**, 5755–5766 (2009).
15. T. D. Ladd, F. Jelezko, R. Laflamme, Y. Nakamura, C. Monroe, and J. L. O'Brien, "Quantum computers," *Nature* **464**, 45–53 (2010).
16. H. Nishihara, M. Haruna, and T. Suhara, *Optical Integrated Circuits* (McGraw-Hill, New York, 1989).
17. B. E. A. Saleh and M. C. Teich, *Fundamentals of Photonics*, 2nd ed. (Wiley, Hoboken, NJ, 2007).
18. A. C. Busacca, C. L. Sones, R. W. Eason, and S. Mailis, "First-order quasi-phase-matched blue light generation in surface-poled Ti:indiffused lithium niobate waveguides," *Appl. Phys. Lett.* **84**, 4430–4432 (2004).
19. Y. L. Lee, C. Jung, Y.-C. Noh, M. Park, C. Byeon, D.-K. Ko, and J. Lee, "Channel-selective wavelength conversion and tuning in periodically poled Ti:LiNbO<sub>3</sub> waveguides," *Opt. Express* **12**, 2649–2655 (2004).
20. S. Tanzilli, H. De Riedmatten, W. Tittel, H. Zbinden, P. Baldi, M. De Michelis, D. B. Ostrowsky, and N. Gisin, "Highly efficient photon-pair source using periodically poled lithium niobate waveguide," *Electron. Lett.* **37**, 26–28 (2001).
21. H. Guillet de Chatellus, A. V. Sergienko, B. E. A. Saleh, M. C. Teich, and G. Di Giuseppe, "Non-collinear and non-degenerate polarization-entangled photon generation via concurrent type-I parametric downconversion in PPLN," *Opt. Express* **14**, 10 060–10 072 (2006).
22. R. C. Alferness and R. V. Schmidt, "Tunable optical waveguide directional coupler filter," *Appl. Phys. Lett.* **33**, 161–163 (1978).
23. R. C. Alferness, "Efficient waveguide electro-optic TE=TM mode converter/wavelength filter," *Appl. Phys. Lett.* **36**, 513–515 (1980).
24. J. Hukriede, D. Runde, and D. Kip, "Fabrication and application of holographic Bragg gratings in lithium niobate channel waveguides," *J. Phys. D: Appl. Phys.* **36**, R1–R16 (2003).
25. D. Runde, S. Brunken, S. Breuer, and D. Kip, "Integrated-optical add/drop multiplexer for DWDM in lithium niobate," *Appl. Phys. B: Lasers Opt.* **88**, 83–88 (2007).
26. D. Runde, S. Breuer, and D. Kip, "Mode-selective coupler for wavelength multiplexing using LiNbO<sub>3</sub>:Ti optical waveguides," *Cent. Eur. J. Phys.* **6**, 588–592 (2008).
27. R. V. Schmidt and H. Kogelnik, "Electro-optically switched coupler with stepped  $\Delta\beta$  reversal using Ti-diffused LiNbO<sub>3</sub> waveguides," *Appl. Phys. Lett.* **28**, 503–506 (1976).
28. H. Kogelnik and R. V. Schmidt, "Switched directional couplers with alternating  $\Delta\beta$ ," *IEEE J. Quantum Electron.* **QE-12**, 396–401 (1976).
29. D. P. DiVincenzo, "Two-bit gates are universal for quantum computation," *Phys. Rev. A* **51**, 1015–1022 (1995).
30. E. Knill, R. Laflamme, and G. J. Milburn, "A scheme for efficient quantum computation with linear optics," *Nature* **409**, 46–52 (2001).
31. M. Fiorentino and F. N. C. Wong, "Deterministic controlled-NOT gate for single-photon two-qubit quantum logic," *Phys. Rev. Lett.* **93**, 070 502 (2004).
32. N. Gisin, S. Pironio, and N. Sangouard, "Proposal for implementing device-independent quantum key distribution based on a heralded qubit amplifier," *Phys. Rev. Lett.* **105**, 070 501 (2010).
33. S. Glancy, H. M. Vasconcelos, and T. C. Ralph, "Transmission of optical coherent-state qubits," *Phys. Rev. A* **70**, 022 317 (2004).
34. D. H. Jundt, "Temperature-dependent Sellmeier equation for the index of refraction,  $n_e$ , in congruent lithium niobate," *Opt. Lett.* **22**, 1553–1555 (1997).
35. K. K. Wong, ed., *Properties of Lithium Niobate* (Institution of Electrical Engineers, Stevenage, U.K., 2002).
36. M. D. Feit, J. A. Fleck, Jr., and L. McCaughan, "Comparison of calculated and measured performance of diffused

- channel-waveguide couplers," J. Opt. Soc. Am. **73**, 1296–1304 (1983).
37. S. K. Korotky and R. C. Alferness, "Ti:LiNbO<sub>3</sub> integrated optic technology," in *Integrated Optical Circuits and Components: Design and Applications*, L. D. Hutcheson, ed. (Marcel Dekker, New York, 1987).
  38. G. B. Hocker and W. K. Burns, "Mode dispersion in diffused channel waveguides by the effective index method," Appl. Opt. **16**, 113–118 (1977).
  39. C. H. Bennett and G. Brassard, "Quantum cryptography: Public key distribution and coin tossing," in *Proceedings of the International Conference on Computers, Systems & Signal Processing*, pp. 175–179 (Institute of Electrical and Electronics Engineers, Bangalore, India, 1984).
  40. A. F. Abouraddy, T. Yarnall, B. E. A. Saleh, and M. C. Teich, "Violation of Bell's inequality with continuous spatial variables," Phys. Rev. A **75**, 052114 (2007).
  41. T. Yarnall, A. F. Abouraddy, B. E. A. Saleh, and M. C. Teich, "Synthesis and analysis of entangled photonic qubits in spatial-parity space," Phys. Rev. Lett. **99**, 250502 (2007).
  42. T. Yarnall, A. F. Abouraddy, B. E. A. Saleh, and M. C. Teich, "Experimental violation of Bell's inequality in spatial-parity space," Phys. Rev. Lett. **99**, 170408 (2007).
  43. B. E. A. Saleh and M. C. Teich, "Sub-Poisson light generation by selective deletion from cascaded atomic emissions," Optics Commun. **52**, 429–432 (1985).
  44. N. Gisin, G. Ribordy, W. Tittel, and H. Zbinden, "Quantum Cryptography," Rev. Mod. Phys. **74**, 145–195 (2002).
  45. A. F. Abouraddy, B. E. A. Saleh, A. V. Sergienko, and M. C. Teich, "Degree of entanglement for two qubits," Phys. Rev. A **64**, 050101 (2001).
  46. P. J. Mosley, J. S. Lundeen, B. J. Smith, P. Wasylczyk, A. B. U'Ren, C. Silberhorn, , and I. A. Walmsley, "Heralded generation of ultrafast single photons in pure quantum states," Phys. Rev. Lett. **100**, 133601 (2008).
  47. Z. H. Levine, J. Fan, J. Chen, A. Ling, and A. Migdall, "Heralded, pure-state single-photon source based on a Potassium Titanyl Phosphate waveguide," Opt. Express **18**, 3708–3718 (2010).
  48. W. P. Grice, A. B. U'Ren, and I. A. Walmsley, "Eliminating frequency and space-time correlations in multiphoton states," Phys. Rev. A **64**, 063815 (2001).
  49. Z. D. Walton, M. C. Booth, A. V. Sergienko, B. E. A. Saleh, and M. C. Teich, "Controllable frequency entanglement via auto-phase-matched spontaneous parametric down-conversion," Phys. Rev. A **67**, 053810 (2003).
  50. Z. D. Walton, A. V. Sergienko, B. E. A. Saleh, and M. C. Teich, "Generation of polarization-entangled photon pairs with arbitrary joint spectrum," Phys. Rev. A **70**, 052317 (2004).
  51. S. Carrasco, J. P. Torres, L. Torner, A. V. Sergienko, B. E. A. Saleh, and M. C. Teich, "Spatial-to-spectral mapping in spontaneous parametric down-conversion," Phys. Rev. A **70**, 043817 (2004).
  52. L. E. Myers, R. C. Eckhardt, M. M. Fejer, R. L. Byer, W. R. Bosenberg, and J. W. Pierce, "Quasi-phase-matched optical parametric oscillators in bulk periodically poled LiNbO<sub>3</sub>," J. Opt. Soc. Am. B **12**, 2102–2116 (1995).
  53. L. L. Buhl and R. C. Alferness, "Ti:LiNbO<sub>3</sub> waveguide electro-optic beam combiner," Opt. Lett. **12**, 778–780 (1987).
  54. Y. Mitsumori, J. A. Vaccaro, S. M. Barnett, E. Andersson, A. Hasegawa, M. Takeoka, and M. Sasaki, "Experimental demonstration of quantum source coding," Phys. Rev. Lett. **91**, 217902 (2003).
  55. A. Yariv, "Coupled-mode theory for guided-wave optics," IEEE J. Quantum Electron. **QE-9**, 919–933 (1973).
  56. A. Djupsjöbacka and B. Lagerstrom, "Stabilization of a Ti:LiNbO<sub>3</sub> directional coupler," Appl. Opt. **28**, 2205–2206 (1989).
  57. F. Lucchi, D. Janner, M. Belmonte, S. Balsamo, M. Villa, S. Giurgola, P. Vergani, and V. Pruneri, "Very low voltage single drive domain inverted LiNbO<sub>3</sub> integrated electro-optic modulator," Opt. Express **15**, 10739–10743 (2007).

## 1. Introduction

We recently investigated the possibility of using spontaneous parametric down-conversion (SPDC) in two-mode waveguides to generate guided-wave photon pairs entangled in mode number, using a cw pump source. If one photon is generated in the fundamental (even) mode, the other will be in the first-order (odd) mode, and *vice versa* [1]. We also considered a number of detailed photonic-circuit designs that make use of Ti:LiNbO<sub>3</sub> diffused channel, two-mode waveguides for generating and separating photons with various combinations of modal, spectral, and polarization entanglement [2]. Selective mode coupling between combinations of adjacent single-mode and two-mode waveguides is a key feature of these circuits.

Although potassium titanyl phosphate (KTiOPO<sub>4</sub>, KTP) single- and multi-mode waveguide structures have also been used for producing spontaneous parametric down-conversion [3–7], it appears that only the generation process, which makes use of a pulsed pump source, has been incorporated on-chip. Substantial advances have also recently been made in the development

of single-mode silica-on-silicon waveguide quantum circuits [8, 9], with an eye toward quantum information processing applications [10–15]. For these materials, however, the photon-generation process necessarily lies off-chip.

Lithium niobate photonic circuits have the distinct advantage that they permit the *generation, transmission, and processing* of photons all to be achieved on a single chip [2]. Moreover, lithium niobate offers a number of ancillary advantages: 1) its properties are well-understood since it is the basis of integrated-optics technology [16]; 2) circuit elements, such as two-mode waveguides and polarization-sensitive mode-separation structures, have low loss [2]; 3) it exhibits an electro-optic effect that can modify the refractive index at rates up to tens of GHz and is polarization-sensitive [17, Sec. 20.1D]; and 4) periodic poling of the second-order nonlinear optical coefficient is straightforward so that phase-matched parametric interactions [18, 19], such as SPDC and the generation of entangled-photon pairs [20, 21], can be readily achieved. Moreover, consistency between simulation and experimental measurement has been demonstrated in a whole host of configurations [22–26]. To enhance tolerance to fabrication errors, photonic circuits can be equipped with electro-optic adjustments. For example, an electro-optically switched coupler with stepped phase-mismatch reversal serves to maximize coupling between fabricated waveguides [27, 28].

Compact photonic circuits with multiple components integrated on a single chip, such as the ones considered here, are likely to be highly important for the efficient implementation of devices in the domain of quantum information science. The Controlled-NOT (CNOT) gate is one such device. It plays an important role in quantum information processing, in no small part because it is a key element in certain sets of universal quantum logic gates (such as CNOT plus rotation) that enable all operations possible on a quantum computer to be executed [11, 15, 29, 30]. Two qubits are involved in its operation: a control and a target. The CNOT gate functions by flipping the target qubit if and only if the control qubit is in a particular state of the computational basis. Two separate photons, or, alternatively, two different degrees-of-freedom of the same photon, may be used for these two qubits. A deterministic, two-qubit, single-photon, CNOT gate was demonstrated using bulk optics in 2004 [31]. More recently, a probabilistic, two-photon, version of the CNOT gate was implemented as a silica-on-silicon photonic quantum circuit; an external bulk-optics source of polarization qubits was required, however [8]. It is worthy of mention that qubit decoherence is likely to be minimal in photonic quantum circuits; however, decoherence resulting from loss in long waveguides can be mitigated by the use of either a qubit amplifier [32] or teleportation and error-correcting techniques [33].

This paper describes a set of basic building blocks useful for manipulating modal qubits in Ti:LiNbO<sub>3</sub> photonic quantum circuits. Section 2 provides a brief description of the geometry and properties of the diffused channel Ti:LiNbO<sub>3</sub> waveguides used in the simulations. Modal qubits are characterized in Sec. 3. Section 4 addresses the coupling of modes between two adjacent waveguides; several special cases are highlighted. The principle of operation of the mode analyzer, which separates the even and odd components of an incoming state into two separate spatial paths, is set forth in Sec. 5, as are the effects of the modal Pauli spin operator  $\sigma_z$ . The mode rotator, which rotates the state by an angle in mode space, is examined in Sec. 6, as is the modal Pauli spin operator  $\sigma_x$ . Section 7 is devoted to describing the design of a deterministic, two-qubit, single-photon, CNOT gate implemented as a Ti:LiNbO<sub>3</sub> photonic quantum circuit, in which the polarization and mode number of a single photon serve as the control and target qubits, respectively. The conclusion is presented in Sec. 8.

## 2. Diffused channel Ti:LiNbO<sub>3</sub> waveguides

All of the simulations presented in this paper refer to structures that make use of Ti:LiNbO<sub>3</sub> diffused channel waveguides, as illustrated in Fig. 1. These waveguides are fabricated by diffusing

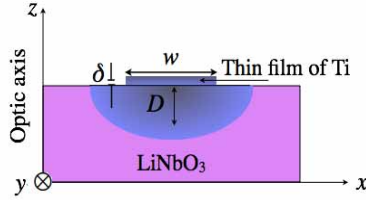


Fig. 1. Cross-sectional view of the fabrication of a diffused channel  $\text{Ti:LiNbO}_3$  waveguide (not to scale). A thin film of titanium of thickness  $\delta \approx 100$  nm and width  $w$  is diffused into a  $z$ -cut,  $y$ -propagating  $\text{LiNbO}_3$  crystal. The diffusion length  $D = 3 \mu\text{m}$ .

a thin film of titanium (Ti), with thickness  $\delta \approx 100$  nm and width  $w$ , into a  $z$ -cut,  $y$ -propagating  $\text{LiNbO}_3$  crystal. The diffusion length  $D$  is taken to be the same in the two transverse directions:  $D = 3 \mu\text{m}$ . The TE mode polarized in the  $x$ -direction sees the ordinary refractive index  $n_o$ , whereas the TM mode polarized in the  $z$ -direction (along the optic axis) sees the extraordinary refractive index  $n_e$ .

The ordinary and extraordinary refractive indices may be calculated by making use of the Sellmeier equations [17, Chap. 5], [34, 35]. The refractive-index increase introduced by titanium indiffusion is characterized by  $\Delta n = 2\delta\rho \operatorname{erf}(w/2D)/\sqrt{\pi}D$ , where  $\rho = 0.47$  and  $0.625$  for  $n_o$  and  $n_e$ , respectively [36]. To accommodate wavelength dispersion,  $\Delta n$  can be modified by incorporating the weak factor  $\xi = 0.052 + 0.065/\lambda^2$ , where the wavelength  $\lambda$  is specified in  $\mu\text{m}$  [37]. We calculate the effective refractive index  $n_{\text{eff}}$  of a confined mode in two ways: 1) by using the effective-index method described in [38]; and 2) by making use of the commercial photonic and network design software package RSoft. The propagation constant of a guided mode is related to  $n_{\text{eff}}$  via  $\beta = 2\pi n_{\text{eff}}/\lambda$ .

Applying a steady electric field to this structure in the  $z$ -direction (along the optic axis) changes the ordinary and extraordinary refractive indices of this uniaxial (trigonal  $3m$ ) material by  $-\frac{1}{2}n_o^3 r_{13} V/d$  and  $-\frac{1}{2}n_e^3 r_{33} V/d$ , respectively [17, Example 20.2-1], where  $V$  is the applied voltage;  $d$  is the separation between the electrodes; and  $r_{13}$  and  $r_{33}$  are the tensor elements of the Pockels coefficient, which have values  $10.9$  and  $32.6 \text{ pm/V}$ , respectively [35].

### 3. Modal qubits

A qubit is a pure quantum state that resides in a two-dimensional Hilbert space. It represents a coherent superposition of the basis states, generally denoted  $|0\rangle$  and  $|1\rangle$ . A qubit can be encoded in any of several degrees-of-freedom of a single photon, such as polarization [39], spatial parity [40], or the mode number of a single photon confined to a two-mode waveguide [1, 2]. The Poincaré sphere provides a geometrical representation for the state of a modal qubit, much as it does for polarization [17, Sec. 6.1A] and spatial parity [41].

Indeed, polarization offers an intrinsically binary basis and is often used to realize a qubit. However, the spatial modes of a photon in a two-mode waveguide, one of which is even and the other odd, are also binary and can therefore also be used to represent a qubit. Modal qubits are particularly suited to photonic quantum circuits since they can be both generated and easily transformed on-chip by making use of elements such as mode analyzers, mode rotators, and two-mode electro-optic directional couplers. The modal space of a two-mode waveguide therefore offers an appealing alternative to polarization for representing qubits in quantum photonic circuits.

The comparison between modal and spatial-parity qubits is instructive. Spatial-parity qubits are defined on a 2D Hilbert space in which the 1D transverse spatial modes of the photon are

decomposed into even and odd spatial-parity components [40–42]. Modal qubits also relate to parity, but in a simpler way. They are defined on a 2D Hilbert space in which the bases are a single 1D even-parity function and a single 1D odd-parity function. These two functions are the fundamental (even,  $m = 0$ ) and first-order order (odd,  $m = 1$ ) transverse spatial eigenmodes of the Helmholtz equation for a two-mode waveguide.

Photon pairs can be exploited for use in quantum photonic circuits [2, 8], as well as for producing heralded single-photon pure states [43] in well-defined spatiotemporal modes, which are required for many quantum information technology applications such as quantum cryptography [44] and linear optical quantum computing [30]. Care must be taken, however, to ensure that the intrinsic quantum correlations between the twin photons are eliminated so that the surviving photon is in a pure state [45–47]. One way of achieving this is to generate the twin photons with a factorable joint amplitude [48–51]. We have previously shown that a Type-0 interaction could be used to generate photon pairs that are degenerate in frequency and polarization, but with opposite mode number [2, Sec. 3]. Coupling these photons into two single-mode waveguides would allow one of these photons to be used to herald the arrival of the other. The heralded photon could then be coupled into a two-mode waveguide which, with the addition of a mode rotator, would serve as a source of modal qubits. Such a source would be analogous to the one fashioned from bulk optics by Fiorentino et al. [31] using Type-II SPDC. However, the Type-0 source of modal qubits described above would be on-chip and would also make use of the strongest nonlinear component of the second-order tensor,  $d_{33}$ , thereby enhancing the efficiency of the interaction [52].

The quantum state of a single photon in a two-mode waveguide, assuming that its polarization is TE or TM, can be expressed as  $|\Psi\rangle = \alpha_1|e\rangle + \alpha_2|o\rangle$ , where  $|e\rangle$  and  $|o\rangle$  represent the even and odd basis states, respectively; and  $\alpha_1$  and  $\alpha_2$  are their weights. All operations on the single-photon state are effected via auxiliary adjacent waveguides, which are sometimes single-mode and sometimes two-mode. We exploit the concepts of selective and controllable coupling between waveguides, together with the isomorphism between waveguide coupling and the SO(2) rotation matrix, to design a mode analyzer, a mode rotator, modal Pauli spin operators, and a CNOT gate useful for quantum information processing.

#### 4. Mode coupling between adjacent waveguides

The coupling between two lossless, single-mode waveguides is described by a unitary matrix  $\mathbf{T}$  that takes the form [17, Sec. 8.5B]

$$\mathbf{T} = \begin{bmatrix} A & -jB \\ -jB^* & A^* \end{bmatrix}, \quad (1)$$

where  $A = \exp(j\Delta\beta L/2)[\cos\gamma L - j(\Delta\beta/2\gamma)\sin\gamma L]$  and  $B = (\kappa/\gamma)\exp(j\Delta\beta L/2)\sin\gamma L$ . Here,  $\Delta\beta$  is the phase mismatch per unit length between the two coupled modes;  $L$  is the coupling interaction length;  $\kappa$  is the coupling coefficient, which depends on the widths of the waveguides and their separation as well as on the mode profiles;  $\gamma^2 = \kappa^2 + \frac{1}{4}\Delta\beta^2$ ; and the symbol \* represents complex conjugation.

This unitary matrix  $\mathbf{T}$  can equivalently be written in polar notation as [53]

$$\mathbf{T} = \begin{bmatrix} \cos(\theta/2)\exp(j\phi_A) & -j\sin(\theta/2)\exp(j\phi_B) \\ -j\sin(\theta/2)\exp(-j\phi_B) & \cos(\theta/2)\exp(-j\phi_A) \end{bmatrix}, \quad (2)$$

where  $\theta = 2\sin^{-1}[(\kappa/\gamma)\sin\gamma L]$ ;  $\phi_A = \phi_B + \tan^{-1}[(-\Delta\beta/2\gamma)\tan\gamma L]$ ; and  $\phi_B = \Delta\beta L/2$ . Using this representation, the coupling between the two waveguides can be regarded as a cascade of three processes: 1) phase retardation, 2) rotation, and 3) phase retardation. This becomes

apparent if Eq. (2) is rewritten as

$$\mathbf{T} = \exp(-j\phi_B) \mathbf{T}_3 \mathbf{T}_2 \mathbf{T}_1, \quad (3)$$

with

$$\mathbf{T}_1 = \begin{bmatrix} 1 & 0 \\ 0 & e^{-j\Gamma_1} \end{bmatrix}; \quad \mathbf{T}_2 = \begin{bmatrix} \cos(\theta/2) & -j\sin(\theta/2) \\ -j\sin(\theta/2) & \cos(\theta/2) \end{bmatrix}; \quad \mathbf{T}_3 = \begin{bmatrix} e^{-j\Gamma_2} & 0 \\ 0 & 1 \end{bmatrix}, \quad (4)$$

where  $\Gamma_1 = \phi_A - \phi_B$ ;  $\Gamma_2 = -\phi_A - \phi_B$ ; and  $\mathbf{T}_1$ ,  $\mathbf{T}_2$ , and  $\mathbf{T}_3$  represent, in consecutive order, phase retardation, rotation, and phase retardation. The phase shift  $\phi_B$  is a constant of no consequence.

For perfect phase matching between the coupled modes, i.e., for  $\Delta\beta = 0$  and an interaction coupling length  $L = q\pi/2\kappa$ , where  $q$  is an odd positive integer, the coupling matrix  $\mathbf{T}$  reduces to

$$\mathbf{T} = \exp\left(\frac{jq\pi}{2}\right) \begin{bmatrix} 0 & -1 \\ -1 & 0 \end{bmatrix}, \quad (5)$$

indicating that the modes are flipped. Applying this operation twice serves to double flip the vector, thereby reproducing the input, but with a phase shift twice that of  $q\pi/2$ . On the other hand, for  $\gamma L = p\pi$ , with  $p$  an integer, the matrix becomes

$$\mathbf{T} = (-1)^p \begin{bmatrix} \exp(j\phi_A) & 0 \\ 0 & \exp(-j\phi_A) \end{bmatrix}. \quad (6)$$

Finally, for weak coupling ( $\kappa \approx 0$  or  $\kappa \ll \Delta\beta$ ), we have  $\phi_A \approx 0$ , whereupon  $\mathbf{T}$  reduces to the identity matrix.

Our interest is in three scenarios: 1) coupling between a pair of single-mode waveguides (SMWs); 2) coupling between a pair of two-mode waveguides (TMWs); and 3) coupling between a SMW and a TMW. The matrix described in Eq. (2) is not adequate for describing the coupling in the latter two cases; in general, a  $4 \times 4$  matrix is clearly required for describing the coupling between two TMWs. However, for the particular cases of interest here, the coupling between the two waveguides is such that only a single mode in each waveguide participates; this is because the phase-matching conditions between the interacting modes are either satisfied — or not satisfied. As an example for identical waveguides, similar modes couple whereas dissimilar modes fail to couple as a result of the large phase mismatch. The net result is that, for the cases at hand, the general matrix described in Eq. (2) reduces to submatrices of size  $2 \times 2$ , each characterizing the coupling between a pair of modes.

## 5. Mode analyzer and modal Pauli spin operator $\sigma_z$

A *mode analyzer* is a device that separates the even and odd components of an incoming state into two separate spatial paths. It is similar to the *parity analyzer* of one-photon parity space [40]. For the problem at hand, its operating principle is based on the selective coupling between adjacent waveguides of different widths. The even and odd modes of a TMW of width  $w_1$  are characterized by different propagation constants. An auxiliary SMW (with appropriate width  $w_2$ , length  $L_2$ , and separation distance  $b_1$  from the TMW) can be used to extract only the odd component [2]. The result is a mode analyzer that separates the components of the incoming state, delivering the odd mode as an even distribution, as shown in Fig. 2(a). The end of the SMW is attached to an S-bend waveguide, with initial and final widths  $w_2$ , to obviate the possibility of further unwanted coupling to the TMW and to provide a well-separated output port for the extracted mode. If it is desired that the output be delivered as an odd distribution

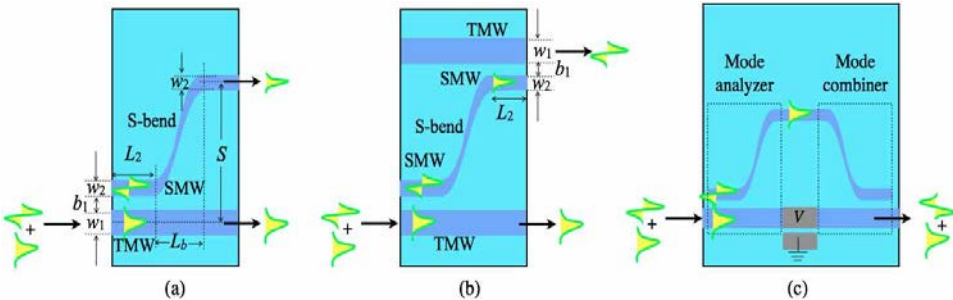


Fig. 2. (a) Sketch of a photonic circuit that serves as a mode analyzer (not to scale). It is implemented by bringing a single-mode waveguide (SMW) of width  $w_2$  and length  $L_2$  into proximity with a two-mode waveguide (TMW) of width  $w_1$ . The two waveguides are separated by a distance  $b_1$ . An S-bend waveguide of initial and final width  $w_2$ , and bending length  $L_b$ , is attached to the end of the SMW. The center-to-center separation between the output of the S-bend and the TMW is denoted  $S$ . All S-bends considered in this paper have dimensions  $L_b = 10$  mm and  $S = 127$   $\mu$ m (the standard spatial separation [26]). The odd mode is separated and delivered as an even distribution. (b) Sketch of a mode analyzer (not to scale) that separates the odd mode and delivers it as an odd distribution. It is more complex than the design presented in (a) because it incorporates a second TMW, again of width  $w_1$ , that is brought into proximity with a SMW of width  $w_2$  and length  $L_2$  placed at the output of the S-bend. These two waveguides are again separated by a distance  $b_1$ . (c) Sketch of a photonic circuit (not to scale) that changes the sign of the odd mode while leaving the even mode intact, thereby implementing the modal Pauli spin operator  $\sigma_z$ . An electro-optic phase modulator is used to compensate for any unintended differences in the phase delays encountered by the even and odd modes as they transit the circuit.

instead, another SMW to TMW coupling region (with the same parameters) may be arranged at the output end of the S-bend, as illustrated in Fig. 2(b). This allows the propagating even mode in the SMW to couple to the odd mode of the second TMW, thereby delivering an odd distribution at the output. The appropriate coupler configuration is determined by the application at hand. It is important to note that the mode analyzer is a bidirectional device: it can be regarded as a *mode combiner* when operated in the reverse direction, as we will soon see.

The Pauli spin (or spatial-parity) operator  $\sigma_z$  introduces a phase shift of  $\pi$  (imparts a negative sign) to the odd component of the photon state, leaving the even component unchanged; it thus acts as a half-wave retarder in mode space. It can be implemented by exploiting modal dispersion between the even and odd modes: a single TMW of length  $\pi/|\beta_e - \beta_o|$ , where  $\beta_e$  and  $\beta_o$  are the propagation constants of the even and odd modes, respectively, results in the desired phase shift of  $\pi$ . For a weakly dispersive medium, however, a waveguide longer than practicable might be required. An alternative approach for implementing the Pauli spin operator  $\sigma_z$  involves cascading a mode analyzer and a mode combiner, as illustrated in Fig. 2(c). As established in Eq. (5), perfect coupling between a pair of adjacent waveguides over an interaction length  $L = q\pi/2\kappa$  introduces a phase shift of  $q\pi/2$ , where  $q$  is an odd positive integer. A cascade of two such couplings thus results in a phase shift  $q\pi$ , with  $q$  odd, thereby implementing the Pauli spin operator  $\sigma_z$ . Proper design dictates that  $\beta_e L_e = \beta_o L_o$ , where  $L_e$  and  $L_o$  are the distances traveled by the even and odd modes, respectively. Imperfections in the fabrication of the circuit may be compensated by making use of an electro-optic (EO) phase modulator, as sketched in Fig. 2(c).

An example illustrating the operation of a mode analyzer, such as that shown in Fig. 2(a), is provided in Fig. 3. The behavior of the normalized propagation constants  $\beta$  of the even

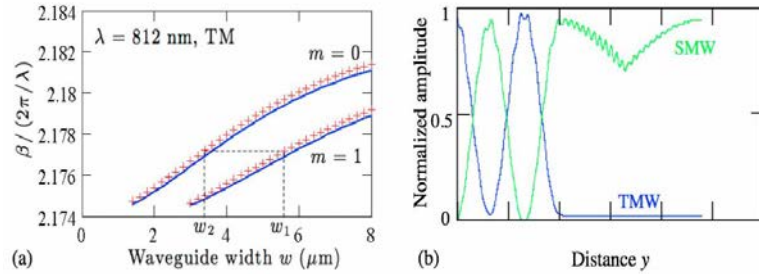


Fig. 3. (a) Dependencies of the normalized propagation constants  $\beta$  of the fundamental ( $m = 0$ ) and first-order ( $m = 1$ ) modes on the widths  $w$  of the diffused channel  $\text{Ti:LiNbO}_3$  waveguides. The input wave has wavelength  $\lambda = 0.812 \mu\text{m}$  and TM polarization. The solid curves were obtained using the effective-index method described in [38], whereas the plus signs were computed using the software package RSoft. The dotted vertical lines represent the desired widths  $w_1$  and  $w_2$ . (b) Simulated performance of a mode analyzer that takes the form displayed in Fig. 2(a). The blue curve represents the evolution with distance of the normalized amplitude of the odd mode in a TMW of width  $w_1 = 5.6 \mu\text{m}$ , whereas the green curve shows the evolution of the even mode in a SMW of dimensions  $w_2 = 3.4 \mu\text{m}$  and  $L_2 = 6.2 \text{ mm}$ . The separation between the TMW and the SMW is  $b_1 = 4 \mu\text{m}$  and the S-bend has dimensions  $L_b = 10 \text{ mm}$  and  $S = 127 \mu\text{m}$ . The dip in the curve for the SMW is associated with the tapered nature of the S-bend. The results were obtained with the help of the software package RSoft.

( $m = 0$ ) and odd ( $m = 1$ ) modes before Ti indiffusion, as a function of the waveguide width  $w$ , is presented in Fig. 3(a) for TM polarization at a wavelength of  $\lambda = 0.812 \mu\text{m}$ . The horizontal dotted line crossing the two curves represents the phase-matching condition for an even and an odd mode in two waveguides of different widths. The simulation presented in Fig. 3(b) displays the evolution of the normalized amplitudes of the two interacting modes with distance.

## 6. Mode rotator and modal Pauli spin operator $\sigma_x$

The *mode rotator* is an operator that rotates the state by an angle  $\theta$  in mode space, just as a polarization rotator rotates the polarization state. It is also analogous to the *parity rotator* of one-photon spatial-parity space [40]. It achieves rotation by cascading a mode analyzer, a *directional coupler*, and a mode combiner; the three devices are regulated by separate EO phase modulators to which external voltages are applied. The mode analyzer splits the incoming one-photon state into its even and odd projections; the directional coupler mixes them; and the mode combiner recombines them into a single output.

Implementation of the mode rotator is simplified by making use of the factorization property of the unitary matrix  $\mathbf{T}$  that characterizes mode coupling in two adjacent waveguides (see Sec. 4). As shown in Eqs. (3) and (4), the coupling between two lossless waveguides can be regarded as a cascade of three stages: phase retardation, rotation, and phase retardation. If the phase-retardation components were eliminated, only pure rotation, characterized by the  $\text{SO}(2)$  operator, would remain.

The phase-retardation components can indeed be compensated by making use of a pair of EO phase modulators to introduce phase shifts of  $\Gamma_1$  and  $\Gamma_2$ , before and after the EO directional coupler, respectively. These simple  $U(1)$  transformations convert  $\mathbf{T}_1$  and  $\mathbf{T}_3$  in Eq. (4) into identity matrices, whereupon Eq. (3) becomes the  $\text{SO}(2)$  rotation operator. For a mode of wavelength  $\lambda$ , and an EO phase modulator of length  $L$  and distance  $d$  between the electrodes, the voltage required to introduce a phase shift of  $\Gamma$  is  $V = \lambda d \Gamma / \pi r n^3 L$ , where the Pockels co-

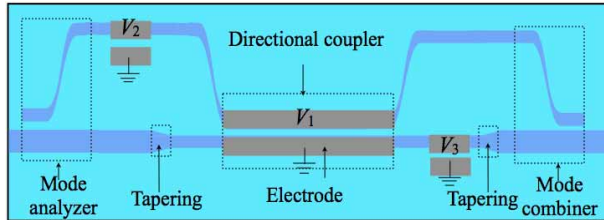


Fig. 4. Sketch of a photonic circuit that serves as a mode rotator (not to scale). It is implemented by sandwiching a directional coupler between a mode analyzer and a mode combiner. The coupling length of the directional coupler is  $\pi/2\kappa$ . To obtain a specified angle of rotation  $\theta$ , voltages  $V_1$ ,  $V_2$ , and  $V_3$  are applied to the EO directional coupler, the input EO phase modulator, and the output EO phase modulator, respectively.

efficient  $r$  assumes the values  $r_{13}$  and  $r_{33}$ , for  $n = n_o$  and  $n = n_e$ , respectively [17, Sec. 20.1B].

The standard EO directional coupler consists of two adjacent identical SMWs and makes use of an EO phase modulator to control the transfer of modal power between them [17, Sec. 20.1D]. When no voltage is applied to the EO modulator, the optical power is totally transferred from one waveguide to the other, provided that the interaction length  $L$  over which they interact is an odd integer multiple of the coupling length,  $\pi/2\kappa$  [17, Sec. 8.5B]. The application of a voltage to the EO modulator introduces a phase mismatch between the two interacting modes that results in partial, rather than full, optical power transfer. In particular, if the voltage is chosen such that  $|\Delta\beta L| = \sqrt{3}\pi$  (or  $\sqrt{7}\pi, \sqrt{11}\pi, \dots$ ), then no power is transferred between the two waveguides. The voltage required to introduce a phase mismatch of  $\Delta\beta$  is approximately  $V = \lambda d \Delta\beta / 2\pi r n^3$  [17, Sec. 20.1D]. The waveguide beam combiner suggested by Buhl and Alferness [53] operates on the same principle.

However, because our modal state resides in a TMW, rather than in a SMW associated with the usual directional coupler, a mode analyzer with a configuration similar to that shown in Fig. 2(a) is used to direct the odd component to one arm of the EO directional coupler, and the even component to the other arm through an adiabatically tapered region, as shown in Fig. 4. A mirror-image tapered region and mode combiner follow the directional coupler to recombine the two components at the output of the device. Voltages  $V_1$ ,  $V_2$ , and  $V_3$  are applied to the EO directional coupler, the input EO phase modulator, and the output EO phase modulator, respectively. The voltages  $V_2$  and  $V_3$  can be modified as necessary to ensure that the overall phases acquired by the odd and even modes, both before and after the directional coupler, are identical when  $V_1 = 0$ .

An example showing the operating voltages  $V_1$ ,  $V_2$ , and  $V_3$  required to obtain a specified angle of rotation  $\theta$  is provided in Fig. 5. The directional-coupler voltage  $V_1$  has an initial value (for  $\theta = 0$ ) that corresponds to a phase mismatch  $|\Delta\beta L| = \sqrt{3}\pi$ ; decreasing  $V_1$  results in increasing  $\theta$ . When  $V_1 = 0$ , the angle of rotation is  $\pi$ ; the device then acts as the Pauli spin operator  $\sigma_x$ , which is a *mode flipper* (analogous to the *parity flipper* [40,41]). For  $V_1 = 0$ , there are an infinite number of solutions for the values of  $V_2$  and  $V_3$ , provided, however, that  $V_2 = -V_3$ .

## 7. Controlled-NOT (CNOT) gate

Deterministic quantum computation that involves several degrees-of-freedom of a single photon for encoding multiple qubits is not scalable inasmuch as it requires resources that grow exponentially [31]. Nevertheless, few-qubit quantum processing can be implemented by exploiting multiple-qubit encoding on single photons [54]. We propose a novel *deterministic, two-qubit, single-photon, CNOT gate*, implemented as a Ti:LiNbO<sub>3</sub> photonic quantum circuit, in which

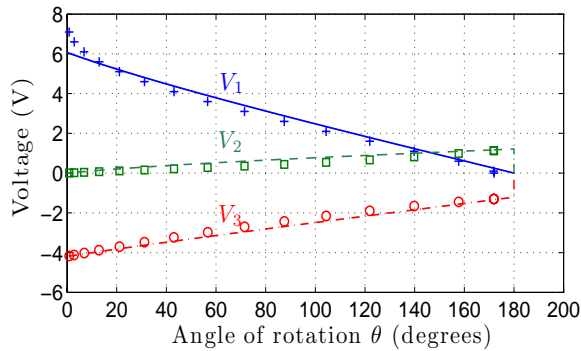


Fig. 5. Operating voltages for the mode rotator vs. the angle of rotation  $\theta$ . Voltages  $V_1$  (solid blue curve),  $V_2$  (dashed green curve), and  $V_3$  (dashed-dotted red curve) are applied to the EO directional coupler, the input EO phase modulator, and the output EO phase modulator, respectively. The input has wavelength  $\lambda = 0.812 \mu\text{m}$  and TM polarization. The directional coupler comprises two identical SMWs separated by  $d = 5 \mu\text{m}$ ; each SMW has width  $2.2 \mu\text{m}$  and length 1.73 mm. The input and output EO phase modulators have electrode lengths of 5 mm and electrode separations of  $5 \mu\text{m}$ . The curves represent theoretical calculations while the symbols represent simulated data obtained using the RSoft program.

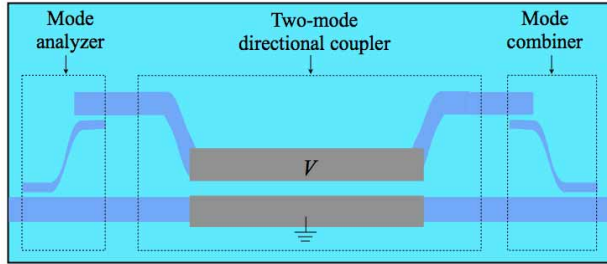


Fig. 6. Sketch of a Ti:LiNbO<sub>3</sub> photonic quantum circuit that behaves as a novel deterministic, two-qubit, single-photon, CNOT gate (not to scale). The control qubit is polarization and the target qubit is mode number. The circuit bears some similarity to the mode rotator shown in Fig. 4; both are implemented by sandwiching an EO directional coupler between a mode analyzer and a mode combiner. However, for the CNOT gate, the EO directional coupler comprises a pair of TMWs, whereas the mode rotator uses a conventional EO directional coupler utilizing a pair of SMWs.

the polarization and mode number of a single photon serve as the control and target qubits, respectively.

The operation of this gate is implemented via a *polarization-sensitive, two-mode, electro-optic directional coupler*, comprising a pair of identical TMWs integrated with an electro-optic phase modulator, and sandwiched between a mode analyzer and a mode combiner. It relies on the polarization sensitivity of the Pockels coefficients in LiNbO<sub>3</sub>. A sketch of the circuit is provided in Fig. 6. The mode analyzer spatially separates the even and odd components of the state for a TM-polarized photon, sending the even component to one of the TMWs and the odd component to the other. At a certain value of the EO phase-modulator voltage, as explained below, the even and odd modes can exchange power. The modified even and odd components are then brought together by the mode combiner.

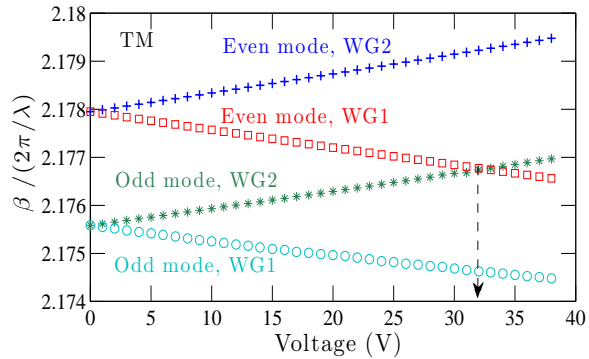


Fig. 7. Dependencies of the normalized propagation constants  $\beta$  on the voltage applied to an EO TMW directional coupler comprising two waveguides [WG1 and WG2]. The propagation constants differ for the even and odd modes except at one particular voltage (vertical dashed line) where the even mode in one waveguide can be phase-matched to the odd mode in the other waveguide. The TMWs are identical, each of width  $4\ \mu\text{m}$ , and they are separated by  $4\ \mu\text{m}$ . The input has wavelength  $\lambda = 0.812\ \mu\text{m}$  and TM polarization. The symbols represent simulated data obtained using the RSoft program.

To show that the device portrayed in Fig. 6 operates as a CNOT gate, we first demonstrate that the target qubit is indeed flipped by a TM-polarized control qubit, so that  $|1\rangle \equiv |\text{TM}\rangle$ . The polarization sensitivity of the Ti:LiNbO<sub>3</sub> TMWs resides in the values of their refractive indices  $n$ , which depend on the polarizations of the incident waves and the voltage applied to its EO phase modulator; and on their Pockels coefficients  $r$ , which depend on the polarization [17, Example 20.2-1]. For a photon with TM polarization, the two-mode EO directional coupler offers two operating regions with markedly different properties. At low (or no) applied voltage, interaction and power transfer take place only between like-parity modes in the two waveguides because the propagation constants of the even and odd modes are different, so they are not phase-matched. However, at a particular higher value of the applied voltage, the behavior of the device changes in such a way that only the even mode in one waveguide, and the odd mode in the other, can interact and exchange power. This arises because the refractive indices of the two waveguides depend on the voltage applied to the device; they move in opposite directions as the voltage increases since the electric-field lines go downward in one waveguide and upward in the other. Figure 7 provides an example illustrating the dependencies of the propagation constants of the even and odd modes, in the two TMWs, as a function of the applied voltage.

At a voltage indicated by the vertical dashed line in Fig. 7, the even mode in one waveguide is phase-matched to the odd mode in the other. In a directional coupler with suitable parameters, a TM-polarized control bit will then result in a flip of the modal bit, whereupon  $\alpha_1|e\rangle + \alpha_2|o\rangle \rightarrow \alpha_1|o\rangle + \alpha_2|e\rangle$ . A TE-polarized control qubit, on the other hand, which sees  $n_o$  rather than  $n_e$ , will leave the target qubit unchanged because of phase mismatch, so that  $|0\rangle \equiv |\text{TE}\rangle$ . Hence, the target qubit is flipped if and only if the control qubit is  $|1\rangle$ , and is left unchanged if the control qubit is  $|0\rangle$ , so that the device portrayed in Fig. 6 does indeed behave as a CNOT gate. In principle, it would also be possible to use a TE-polarized control qubit to flip the target bit; this option was not selected because it would require a higher value of EO phase-modulator voltage since the TE Pockels coefficient  $r_{13}$  is smaller than the TM Pockels coefficient  $r_{33}$  [35].

A drawback of the photonic circuit illustrated in Fig. 6 is that it suffers from the effects of dispersion, which is deleterious to the operation of circuits used for many quantum informa-

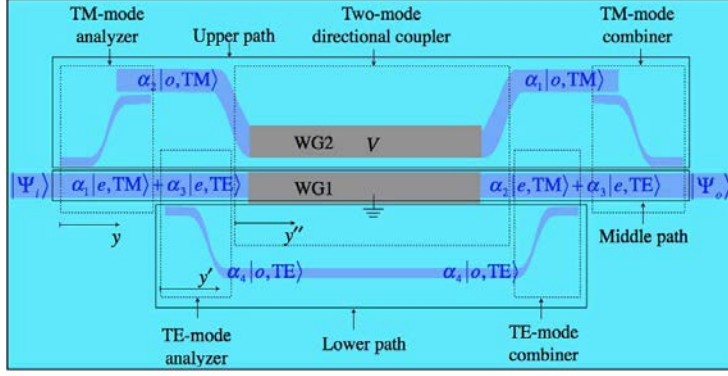


Fig. 8. Sketch of a Ti:LiNbO<sub>3</sub> photonic quantum circuit that behaves as a novel dispersion-managed, deterministic, two-qubit, single-photon, CNOT gate (not to scale). The control qubit is polarization and the target qubit is mode number. The design is more complex than that shown in Fig. 6 because it accommodates dispersion management via path-length adjustments of the upper, middle, and lower paths. An EO TMW directional coupler is sandwiched between polarization-sensitive mode analyzers and polarization-sensitive mode combiners. The lower and upper waveguides of the two-mode directional coupler are denoted WG1 and WG2, respectively. The paths taken by the components of the input state  $|\Psi_i\rangle$  are shown, as is the output state  $|\Psi_o\rangle$ .

tion applications. Dispersion results from the dependence of the propagation constant  $\beta$  on frequency, mode number, and polarization. Polarization-mode dispersion generally outweighs the other contributions, especially in a birefringent material such as LiNbO<sub>3</sub>.

Fortunately, however, it is possible to construct a photonic circuit in which the phase shifts introduced by dispersion can be equalized. A Ti:LiNbO<sub>3</sub> photonic quantum circuit that behaves as a novel dispersion-managed, deterministic, two-qubit, single-photon, CNOT gate is sketched in Fig. 8. It makes use of three paths (upper, middle, and lower), in which the path-lengths of the three arms are carefully adjusted to allow for dispersion management. The third path provides the additional degree-of-freedom that enables the optical path-lengths to be equalized.

The design relies on the use of polarization-dependent mode analyzers at the input to the circuit. The TM-mode analyzer couples the odd-TM component of the state to the upper path, while the TE-mode analyzer couples the odd-TE component to the lower path. The even-TM and even-TE components continue along the middle path. Polarization-dependent mode combiners are used at the output of the circuit.

If the control qubit is in a superposition state, the general quantum state at the input to the circuit, which resides in a 4D Hilbert space (2D for polarization and 2D for mode number), is expressed as

$$\begin{aligned} |\Psi_i\rangle &= \alpha_1|e, \text{TM}\rangle + \alpha_2|o, \text{TM}\rangle + \alpha_3|e, \text{TE}\rangle + \alpha_4|o, \text{TE}\rangle \\ &= |\text{TM}\rangle \otimes [\alpha_1|e\rangle + \alpha_2|o\rangle] + |\text{TE}\rangle \otimes [\alpha_3|e\rangle + \alpha_4|o\rangle] \\ &= |e\rangle \otimes [\alpha_1|\text{TM}\rangle + \alpha_3|\text{TE}\rangle] + |o\rangle \otimes [\alpha_2|\text{TM}\rangle + \alpha_4|\text{TE}\rangle], \end{aligned} \quad (7)$$

where  $|e\rangle$  and  $|o\rangle$  are the basis states of the modal subspace;  $|\text{TM}\rangle$  and  $|\text{TE}\rangle$  are the basis states of the polarization subspace; the  $\alpha$ 's represent the basis weights; and  $\otimes$  indicates the tensor product. Since the target (modal) qubit is flipped by a TM control qubit, the output state  $|\Psi_o\rangle$

becomes

$$\begin{aligned} |\Psi_o\rangle &= \alpha_1|o, \text{TM}\rangle + \alpha_2|e, \text{TM}\rangle + \alpha_3|e, \text{TE}\rangle + \alpha_4|o, \text{TE}\rangle \\ &= |\text{TM}\rangle \otimes [\alpha_1|o\rangle + \alpha_2|e\rangle] + |\text{TE}\rangle \otimes [\alpha_3|e\rangle + \alpha_4|o\rangle], \end{aligned} \quad (8)$$

where it is clear that the two terms in the input state,  $\alpha_1|e, \text{TM}\rangle$  and  $\alpha_2|o, \text{TM}\rangle$ , are converted to  $\alpha_1|o, \text{TM}\rangle$  and  $\alpha_2|e, \text{TM}\rangle$ , respectively, at the output, exemplifying the operation of this CNOT gate. Figure 8 displays the paths taken by the components of the input state provided in Eq. (7); the output state set forth in Eq. (8) is also indicated.

The output state in Eq. (8) is entangled in polarization and mode number; it is inseparable and cannot be written in factorizable form. A particular property of the CNOT gate is the induction of entanglement between factorized qubits: if the control qubit is in the superposition state  $\frac{1}{\sqrt{2}}[|\text{TM}\rangle + |\text{TE}\rangle]$ , and the target qubit is in one of the computational basis states, then the output state of the CNOT gate is maximally entangled. An experimental test of the entanglement created between the polarization and modal degrees-of-freedom can be effected by using quantum-state tomography. The input to the CNOT gate can be readily generated from a product state, say  $|\text{TM}\rangle \otimes |e\rangle$ , by rotation using a waveguide-based EO TE=TM mode converter [23, 55], in addition to a phase modulator, as described in Sec. 6.

It remains to demonstrate the manner in which dispersion management can be achieved in the CNOT gate displayed in Fig. 8. The phase shift  $\varphi$  acquired by each component at the output is given by

$$\begin{aligned} \varphi_{e, \text{TM}} &= \beta_{e, \text{TM}} \ell_1 + \beta_{o, \text{TM}} \ell_2 + \beta' L_D - (2q_1 + q_2)\pi/2 \\ \varphi_{o, \text{TM}} &= \varphi_{e, \text{TM}} \\ \varphi_{e, \text{TE}} &= 2\beta_{e, \text{TE}} \ell_1 + \beta'' L_D \\ \varphi_{o, \text{TE}} &= 2\beta_{o, \text{TE}} \ell_3 - q_3\pi + 2\phi_A, \end{aligned} \quad (9)$$

where the  $\beta$ 's are the mode propagation constants;  $\beta'$  is the propagation constant of either the TM-even mode in WG1 or the TM-odd mode in WG2;  $\beta''$  is the propagation constant of the TE-even mode in WG1;  $q_1$ ,  $q_2$ , and  $q_3$  are odd positive integers that depend on the lengths of the TM-mode analyzer, directional coupler, and TE-mode analyzer, respectively;  $L_D$  is the length of the directional-coupler electrode;  $\ell_1$  is the path-length for the even modes before and after the directional coupler,  $\ell_2$  is the path-length for the odd-TM mode before and after the directional coupler; and  $2\ell_1 + L_D$ ,  $2\ell_2 + L_D$ , and  $2\ell_3$  are the overall physical lengths of the middle, upper, and lower paths, respectively. The phase shift  $\phi_A$  arises from the coupling that affects the odd-TE component as it travels through the TM-mode analyzer. Phase shifts that accrue for the even modes as they pass through the mode analyzers and mode combiners are neglected because of large phase mismatches and weak coupling coefficients. By adjusting the lengths  $\ell_1$ ,  $\ell_2$ , and  $\ell_3$ , we can equalize the phase shifts encountered by each component of the state. Imperfections in the fabrication of the circuit may be compensated by making use of EO phase modulators.

A simulation that demonstrates the performance of the polarization-dependent mode analyzers and EO TMW directional coupler is presented in Fig. 9. The lengths  $\ell_1$ ,  $\ell_2$ , and  $\ell_3$  are assumed to be adjusted such that they equalize the phase shifts encountered by each component of the state so that dispersion is not an issue. The spatial evolution of the normalized amplitudes of the odd and even modes inside the TM-mode analyzer, for TM- and TE-polarization, are displayed in Figs. 9(a) and 9(b), respectively. It is apparent that the TM-mode analyzer extracts only the TM-odd component, while the TE-odd component remains in the TMW waveguide until it couples to the lower path via the TE-mode analyzer [see Fig. 9(c)]. Figures 9(d), (e), and (f) display the performance of the directional coupler for modal inputs that are TM-even, TM-odd, and TE-even, respectively. It is apparent in Fig. 9(d) that the power in the even mode in WG1 is transferred to the odd mode in WG2 for TM polarization. Figure 9(e) reveals comple-

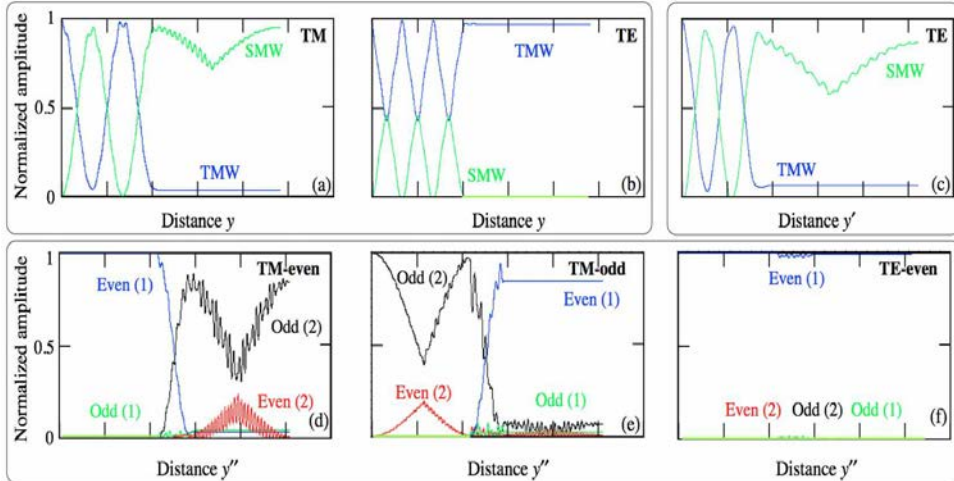


Fig. 9. Simulation demonstrating the performance of the polarization-dependent mode analyzers and the EO TMW directional coupler associated with the dispersion-managed, deterministic, two-qubit, single-photon, CNOT gate set forth in Fig. 8. The input wavelength is  $\lambda = 0.812 \mu\text{m}$ . The TM-mode-analyzer and mode-combiner parameters are  $w_1 = 5.6 \mu\text{m}$ ,  $w_2 = 3.4 \mu\text{m}$ ,  $b_1 = 4 \mu\text{m}$ , and  $L_2 = 6.2 \text{ mm}$ ; the TE-mode-analyzer and mode-combiner parameters are  $w_2 = 3 \mu\text{m}$ ,  $b_1 = 4 \mu\text{m}$ , and  $L_2 = 3.7 \text{ mm}$  (see Fig. 2 for symbol definitions). The S-bends have dimensions  $L_b = 10 \text{ mm}$  and  $S = 127 \mu\text{m}$ . The TMW directional-coupler has length  $L_1 = 2.2 \text{ mm}$ , waveguide width  $w_1 = 5.6 \mu\text{m}$ , electrode separation  $d = 4 \mu\text{m}$ , and an EO phase-modulator voltage  $V = 36 \text{ V}$  applied to WG2, with WG1 at ground potential. All panels display the spatial evolution of the normalized amplitudes of the interacting modes. (a) The curves display strong coupling between the odd and even modes for TM-polarization inside the TM-mode analyzer. The input odd mode in the TMW is shown in blue and the even mode transferred to the SMW is shown in green [the same color conventions are used in panels (b) and (c)]. The even mode is ultimately coupled to another TMW at the output of the TM-mode analyzer and once again becomes odd. (b) The curves show negligible coupling between the odd and even modes for TE-polarization inside the TM-mode analyzer. (c) The curves display good coupling between the odd and even modes for TE-polarization inside the TE-mode analyzer. At the TE-mode combiner, the even mode in the SMW once again becomes an odd mode in the TMW. Panels (d), (e), and (f) display the performance of the directional coupler for modal inputs that are TM-even, TM-odd, and TE-even, respectively. For a given polarization, the blue and green curves represent the amplitudes of the even [denoted Even(1)] and odd [denoted Odd(1)] modes in WG1, respectively, while the red and black curves are the amplitudes of the even [denoted Even(2)] and odd [denoted Odd(2)] modes in WG2, respectively. All simulated data in this figure were obtained using the RSoft program.

mentary behavior: the power in the odd mode in WG2 is transferred to the even mode in WG1. Figure 9(f), on the other hand, shows that the TE-even mode travels through the directional coupler with essentially no interaction. Figures 9(d), (e), and (f), taken together, along with the observation that the TE-odd mode preserves its modal profile during propagation, demonstrate a flip of the modal target qubit by the TM-polarized control qubit, and no flip by a TE-polarized control qubit, confirming that the photonic circuit in Fig. 8 behaves as a CNOT gate.

The absence of a total power transfer from one waveguide to another in Figs. 9(d) and 9(e) can be ascribed to sub-optimal simulation parameters. The conversion efficiency can be expected to improve upon: 1) optimizing the length of the two-mode directional coupler; 2) minimizing bending losses by increasing the length of the S-bend; 3) mitigating the residual phase mismatch by more careful adjustment of the voltage; and 4) improving numerical accuracy. Moreover, the deleterious effects of dc drift and temperature on the operating voltage and stability of the two-mode directional coupler can be minimized by biasing it via electronic feedback [56]; a novel technique based on inverting the domain of one of its arms can also be used to reduce the required operating voltage [57]. Finally, it is worthy of note that decoherence associated with the use of a cascade of CNOT gates, such as might be encountered in carrying out certain quantum algorithms, may be mitigated by the use of either a qubit amplifier [32] or teleportation and error-correcting techniques [33].

## 8. Conclusion

The modes of a single photon in a two-mode Ti:LiNbO<sub>3</sub> waveguide have been co-opted as basis states for representing the quantum state of the photon as a modal qubit. Various photonic quantum circuit designs have been presented for carrying out basic operations on modal qubits for quantum information processing applications. These include a mode analyzer, a mode rotator, and modal Pauli spin operators. We have also described the design of a deterministic, two-qubit, single-photon, CNOT gate, as well as a dispersion-managed version thereof, that rely on a single photon with both modal and polarization degrees-of-freedom in a joint 4D Hilbert space. The CNOT gate is a key element in certain sets of universal quantum logic gates. Simulations of the performance of all of these components, carried out with the help of the commercial photonic and network design software package RSoft, provide support that they operate as intended. The design of these devices is based on selective and controllable power coupling among waveguides, the isomorphism between waveguide coupling and the SO(2) rotation matrix, and the tensor polarization properties of the Pockels coefficients in lithium niobate. The flexibility of Ti:LiNbO<sub>3</sub> as a material for the fabrication guided-wave structures should accommodate the development of increasingly complex quantum circuits and serve to foster new architectures.

## Acknowledgments

This work was supported by the Bernard M. Gordon Center for Subsurface Sensing and Imaging Systems (CenSSIS), an NSF Engineering Research Center; by a U.S. Army Research Office (ARO) Multidisciplinary University Research Initiative (MURI) Grant; and by the Boston University Photonics Center.